Electric Force Microscopy Characterization of Buried Graphitic Channels Microfabricated by MeV Ion Beam Implantation

E. Bernardi[1,2,3], A. Battiato[1,2,3], L. La Torre[4], P. Olivero[1,2,3], F. Picollo[1,2,3], V. Rigato[4], E. Vittone[1,2,3].

[1] *Dipartimento di Fisica, University of Torino, Torino, Italy.* [2] *NIS Centre of Excellence, University of Torino, Torino, Italy.*
[3] *INFN Sezione di Torino, Torino, Italy.* [4] *INFN, Laboratori Nazionali di Legnaro, Legnaro (Padova), Italy.*

INTRODUCTION

MeV ion beam implantation is an effective tool to microfabricate graphitic structures buried inside the diamond crystal. Since the process of damage induced by energetic (MeV) ion is not uniform, a high density of vacancies is mainly introduced few micrometers below the sample surface promoting the amorphization of that region. After high temperature thermal treatments the amorphous layer converts to graphite while the cap layer (i.e. the low-damaged region) restores its diamond structure.

The use of variable-thickness masks on the diamond surface allows the tuning of the ion penetration depth in order to realize channels with emerging endpoints, with promising applications in radiation detection and bio-sensing [1,2].

In the present paper we report about the Electric Force Microscopy (EFM) characterization of these buried graphitic channels.

GRAPHITIC CHANNEL MICROFABRICATION

Ion Implantation is performed on a synthetic single-crystal diamond that is produced by HPHT (High Pressure High Temperature) process, it is classified as type Ib due its contents of substitutional nitrogen ([N] ~10 ÷ 100 ppm). The crystal is cut along the [100] plane and it is polished only on one large face.

The sample was implanted at the AN2000 accelerator of the INFN - Legnaro National Laboratories with a focused 1.2 MeV He^+ ion beam at fluence of ~1×10^{17} cm^{-2}. The beam spot size was ~10 µm and the beam current was comprised between 2 and 3 nA.

Before the implantation process, three quadrants of diamond's surface were covered with a copper layer in order to reduce the ion penetration depth without modifying the beam energy: two quadrants were covered with a 1 µm thick layer and a quadrant was covered with a 0.5 µm thick layer, while the fourth quadrant was not metalized. After this step, further metal deposition of variable-thickness masks was realized in order to implant channels with emerging end-points [3-6].

Four structures were realized: two channels were implanted on the uncovered quadrant creating highly-damaged layers ~2 µm below the surface; a second channel was implanted through the 0.5 µm thick layer resulting in the formation of damaged layers at ~1.5 µm depth; finally, one shallow channel was created 1 µm below the sample surface by implantation through the 1 µm layer. Figure 1a shows a schematic of the sample in which the metal depositions and the channels position are indicated while the geometry of channels emersion due to variable-thickness masks is shown in figure 1b.

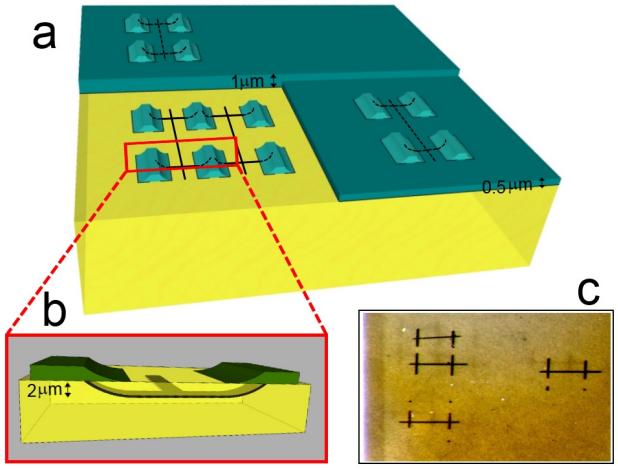

Fig. 1. a) schematic of sample in which black lines represent the graphitic channels and the green structures are the metal depositions (not in scale); b) cross-section of channel and variable thickness mask; c) optical micrograph of implanted diamond after thermal treatment.

Thermal annealing at 900 °C for 1 hour was performed in order to induce the graphitization of the highly-damaged buried region. An optical micrograph of the channels after the thermal treatment is shown in figure 1c.

Finally, the channels end-points were provided with metal pads: a Cr/Cu deposition was followed by 400 °C heating for 1 hour in order to create a conductive carbide compound with chromium. Here we report on the EFM characterization of the 1-µm-deep channel.

EFM CHARACTERIZATION

One end of the channel was kept at a bias voltage with a Keithley 614 electrometer used as a voltage source. A Park Scientific XE-100 Atomic Force Microscope (AFM) and rectangular Au-Cr-coated cantilevers (NSC-14 Cr-Au, MikroMash) were used for this study. Cantilevers have a spring constant around 5.7 N m^{-1}, and resonance frequency

between 160 and 170 kHz. The AFM topological maps (both amplitude and phase signals) and the EFM maps (amplitude signal) were simultaneously recorded in non-contact mode. The frequency of vibration of the cantilever was fixed to a value slightly above its resonance frequency. Electrostatic forces were detected at lock-in frequency ω = 17 kHz. The *ac* voltage applied to the cantilever tip was set to V_{ac} = 2.5 V.

The typical scanning area was 35×35 μm^2 at a scanning rate of 0.5 Hz. All measurements were performed at room temperature.

The EFM amplitude image is constructed from the first-harmonic (ω) component of the force between tip and sample surface [7]. In general, this force is a combination of electrostatic and capacitive forces:

$$F_{1\omega} = Q_t E_s + \frac{\partial C_t}{\partial z}(V_{dc} - V_s)V_{ac} \; ; \qquad (1)$$

where C_t is the capacitance of the tip–surface configuration, $Q_t = C_t \cdot V_{ac}$ is the charge induced on the tip, E_s is the electrostatic field due to the fixed charges on the sample surface, dC_t/dz is the derivative of the tip–surface capacitance with respect to tip–surface distance, V_{dc} and V_{ac} are respectively the *dc* and *ac* voltages applied to the tip, and V_s is the surface potential. In our set-up the *dc* voltage was applied to the buried channel.

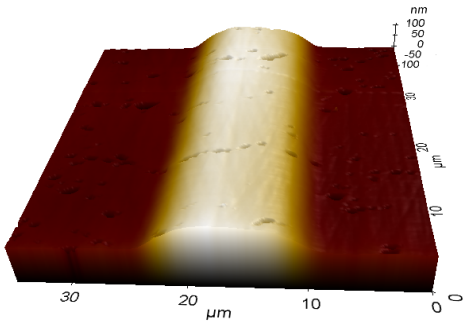

Fig. 2. AFM 3D topography image of the diamond surface above the 1 μm deep channel.

The AFM topography map and 3D reconstruction of the diamond surface above the channel are reported respectively in figure 2.

It can be noted that a pronounced swelling of ~100 nm is localized at the implanted area. This is a well know effect [8] due the lower density of the graphite channel with respect to the diamond's one.

Figure 3a shows the EFM amplitude image taken with an applied voltage to the buried channel of V_{dc} = +3.5 V, while figure 3b refers to an applied voltage of V_{dc}= –3.5 V.

In figure 3c we report a comparison between the EFM amplitude profiles along the horizontal axis in figure 3a and 3b for the two different values of V_{dc}. The profiles were averaged along the vertical axis to improve signal statistics.

There are three factors contributing to the EFM signal (see equation 1): i) the potential difference between the tip and sample, ii) the capacitance of the tip-sample configuration and iii) the electrostatic interaction between the tip and fixed charges on the sample surface.

The electrostatic contribution can be excluded as source of the contrast in figure 3a and 3b because the difference between the EFM amplitude signal directly above the buried channel and the EFM amplitude signal outside this region strongly depends on the absolute value of V_{dc}.

Regarding the other two contributions, the signal contrast must be attributed to a capacitance variation, because EFM images taken by reversing the polarization are similar and not strictly complementary (see figure 3c) [9].

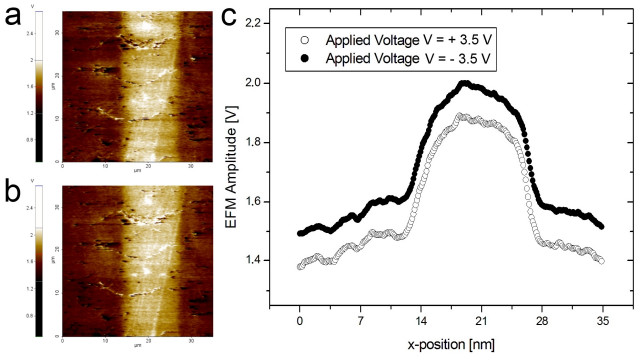

Fig. 3. EFM amplitude maps of the diamond surface above the channel. The voltages applied to the channel with respect to the tip are V_{dc} = +3.5 V (a) and V_{dc} = –3.5 V (b). c) comparison between EFM profiles acquired at V_{dc} = +3.5 V e V_{dc} = –3.5 V. Profiles are averaged along the vertical axis in figure 3a and 3b in order to improve the signal statistics.

CONCLUSIONS

The preliminary results presented in this paper indicate that Electric Force Microscopy is a insightful technique to probe buried graphitic channels in diamond. Future activities will be focused on characterize the other channels implanted at different depths and in different voltage configurations.

[1] J. Forneris et al., Nucl. Instr. Meth. Phys. Res. B, DOI: 10.1016/j.nimb.2012.12.056, in press (2013).
[2] F. Picollo et al., Adv. Mater., accepted for publication (2013).
[3] P. Olivero et al., Diamond Relat. Mater. 18 (2009) 870.
[4] P. Olivero et al., Eur. Phys. J. 75 (2010) 127.
[5] F. Picollo et al., Diamond Relat. Mater. 19 (2010) 466.
[6] F. Picollo et al., New J. Phys. 14 (2012) 053011.
[7] F. Saurenbach and B. D. Terris, Appl. Phys. Lett. 56 (1990) 1703.
[8] F. Bosia et al., Nucl. Instr. Meth. B 268 (2010) 2991.
[9] L. Yonghua et al., Phys. Rev. Lett. 97 (2006) 076805.